PROJECT ECHO

Receiving System

By E. A. OHM

(Manuscript received April 10, 1961)

A tracking horn-reflector antenna, a maser preamplifier (or standby parametric preamplifier), and a special FM demodulator were combined to form a low-noise receiving system which was used to achieve a high-quality voice circuit via the Echo I passive satellite. This paper describes the 2390-mc receiving system located at Holmdel, New Jersey.

I. INTRODUCTION

By using large antennas and a high-powered transmitter, it was calculated that a modest carrier could be received in New Jersey from California via the Echo I satellite.[1] In order to establish a good voice circuit with this carrier, it was clear that the effects of noise had to be reduced by using a very-low-noise receiver. It was also clear that a special demodulator, which featured FM with negative feedback,[2] could reduce the noise effects still further. Although a parametric amplifier in combination with this type of demodulator would yield a good voice circuit under near-ideal conditions, a maser would allow a circuit with a more practical carrier-to-noise margin.* In this regard, a previous experiment had demonstrated that an ultra-low-noise system temperature could be achieved in practice by using a low-noise horn-reflector antenna in combination with a traveling-wave solid state maser.[3] In accordance with these preliminary results, a larger horn-reflector tracking antenna was combined with two traveling-wave masers or alternately two "standby" parametric amplifiers to provide two separate low-noise systems, one for each sense of circular polarization. Special FM demodulators were used to achieve voice circuits of excellent quality from the resulting modest

* It is important to maintain some margin; otherwise, at a critical carrier-to-noise ratio a small decrease in carrier or increase in noise will change the voice circuit from one that sounds good to one that is completely unintelligible. A discussion of this "threshold" effect is included in a companion paper by Ruthroff.[2] For the 3-kc audio circuit used here, the "threshold" ratio of carrier to noise power (referred to a 6-kc band) is 14 db.

carrier-to-noise ratios. In addition, AGC voltages from the FM demodulator were used to monitor the carrier levels, voltages proportional to the system temperatures but independent of incoming carrier levels were derived, and each of these voltages was recorded and calibrated. The discussion also points out how certain measuring and operating techniques were used to obtain the most accurate experimental results.

Section II describes how the receiver generated useful output information. It is followed by sections on the system noise temperature, the FM demodulator AGC characteristics, and the experimental results.

II. RECEIVER DESCRIPTION

A block diagram of the receiving system is shown in Fig. 1. Its operation will be explained by describing how each successive block acts on the carrier and/or noise as it passes through the receiver. (The italicized words in this section refer to blocks labeled in Fig. 1.)

Starting on the left it is assumed that both senses of circularly polarized carrier and noise powers are incident on the antenna. A special significance of the *sky* is that thermal radiation from the atmosphere increases the system noise temperature (as indicated in Fig. 2) as the antenna is lowered toward the horizon. The *horn antenna* focuses the circularly

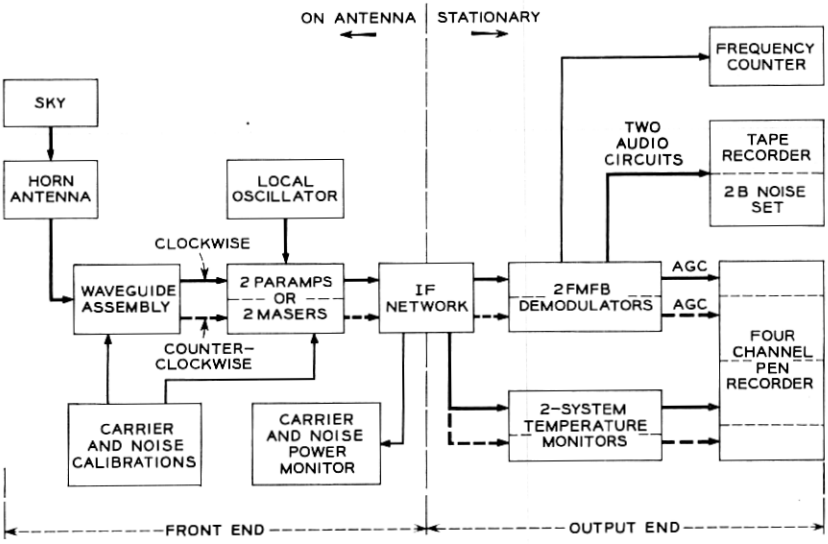

Fig. 1 — Block diagram of Holmdel receiver.

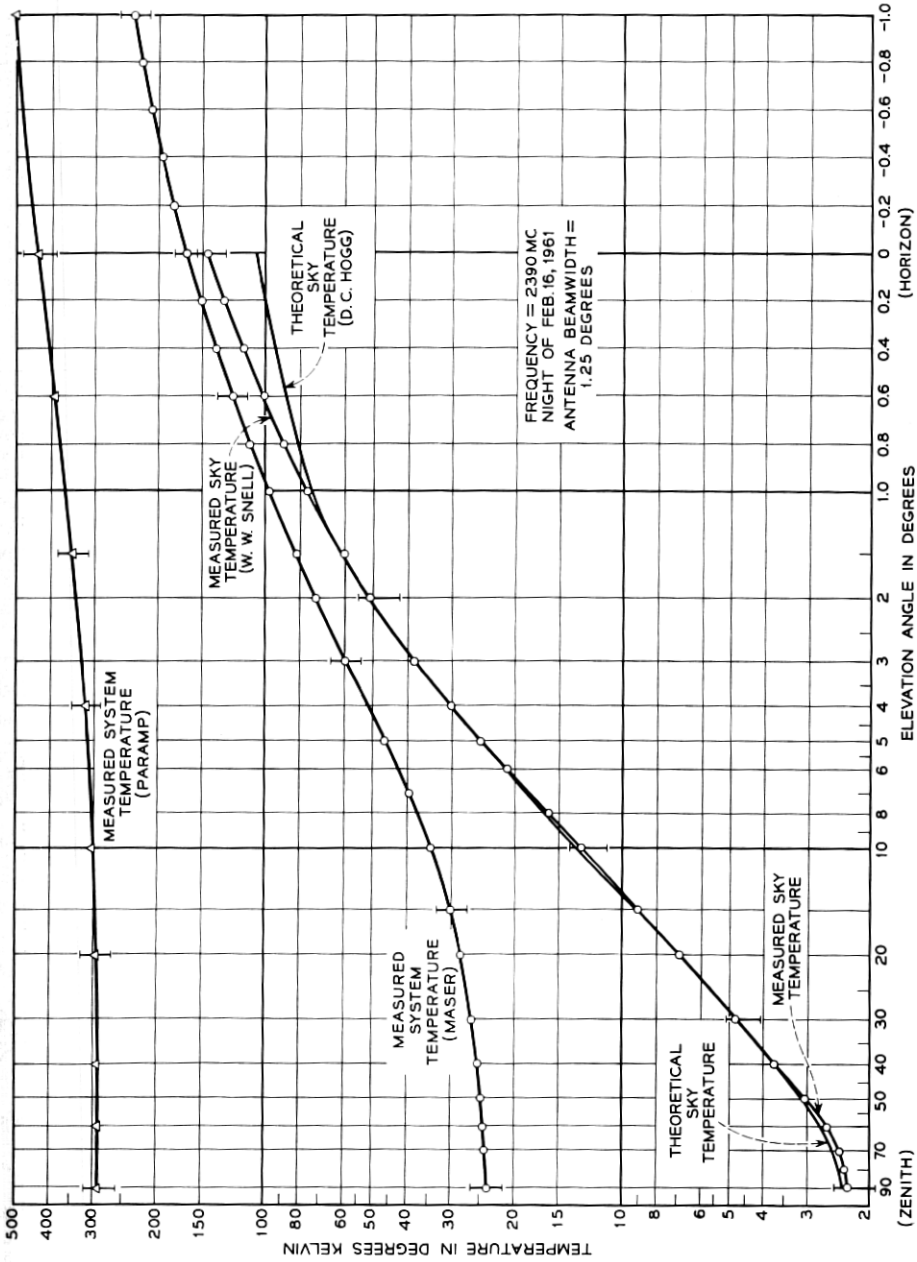

Fig. 2 — Measured sky and system temperatures.

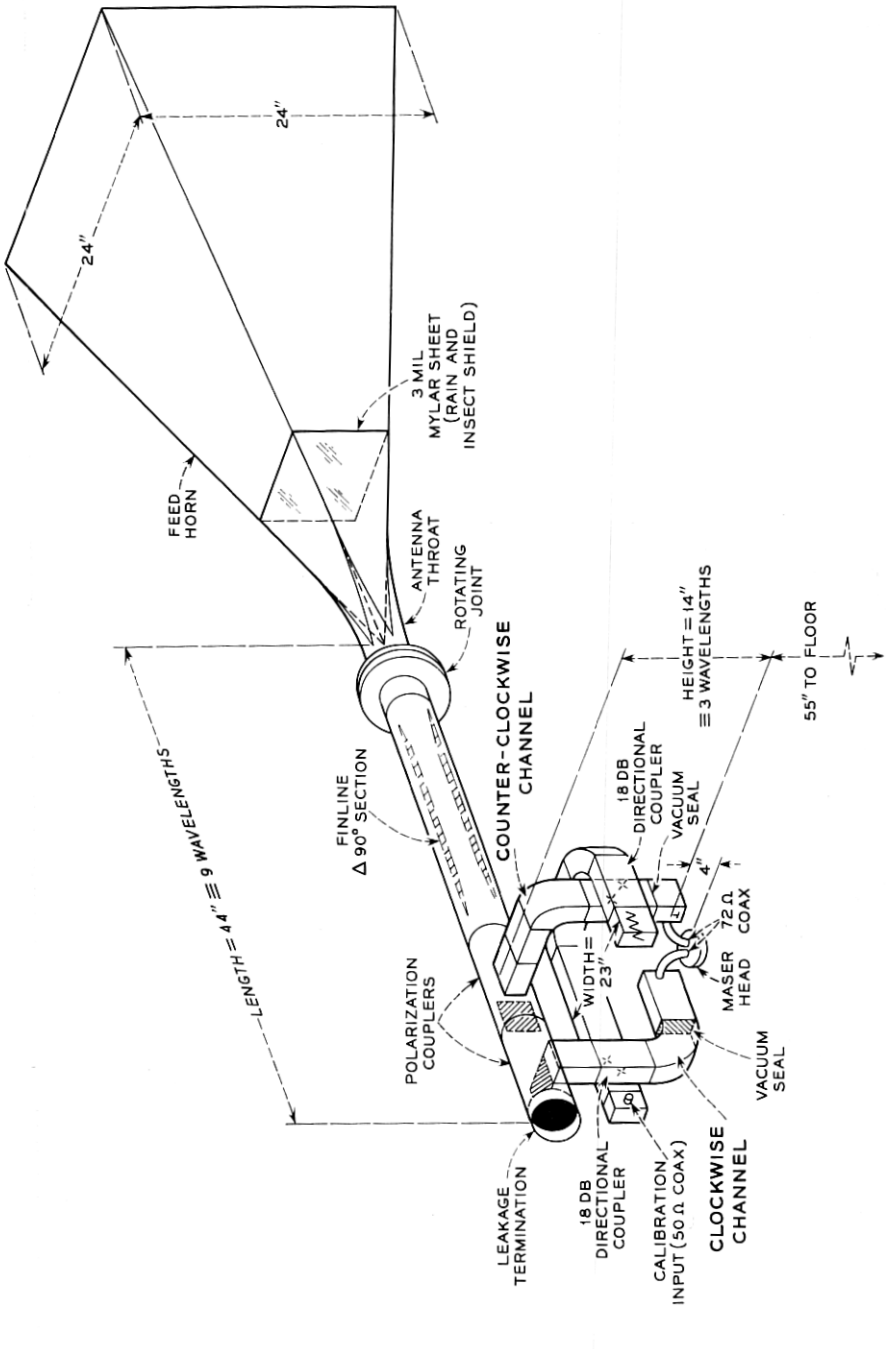

Fig. 3 — Waveguide assembly.

polarized carriers and noise into the *waveguide assembly*, which is shown in Fig. 3. There, after passage through a rotating joint, the finline $\Delta 90°$ section converts the two senses of circular polarizations into orthogonal linear polarizations, and these are further separated by the polarization couplers into separate waveguide channels. These are indicated as the "clockwise" and "counter-clockwise" channels in Fig. 3. Two 18-db waveguide directional couplers are also provided in this region for the convenient insertion of *carrier and noise calibrations* into each channel. From here the two channels are connected via waveguide-to-coaxial transducers to two *maser preamplifiers* or alternatively to two *parametric preamplifiers*. From this point on the channels are completely alike and independent, and therefore only one of them will be discussed.

After sufficient preamplification to nearly eliminate the effects of the noise from the following stages, the carrier and noise powers are heterodyned with a *local oscillator* to an intermediate frequency. The *IF network* further amplifies the carrier and noise to reduce the effects of possible interference, and then transmits this information via the antenna slip ring assembly and long runs of coaxial cable to the "output end" of the receiver. A means for bridging the antenna end of either IF transmission line with a *carrier and noise power monitor* is also provided, so that the "front end" of each channel can be readily tuned and its system temperature measured from inside the antenna cab.

One output of each IF transmission line is connected to an *FM with negative feedback* (*FMFB*) *demodulator*. This unit recovers the audio modulation from the frequency modulated carrier with the usual FM advantage, but for a much smaller carrier-to-noise ratio than otherwise possible. For proper demodulation over a wide range of 70-mc carriers, the 1.2-mc input of the FM limiter is held constant with an AGC feedback loop, which is shown in Fig. 3 of Ref. 2. A sample of this AGC voltage is forwarded to the *recorder*, where a back bias is superimposed to display the voltage range of greatest interest. By adding known 2390-mc carrier powers to the RF input of each channel (via the 18-db waveguide directional couplers) it was practical to calibrate AGC carrier level voltages before and after every pass. Typical recorded AGC voltages are shown in Fig. 4, where they are labeled "counter-clockwise channel carrier" (top recording) and "clockwise channel carrier" (third from top).*

Thus far it has been tacitly assumed that the carrier and noise bandwidths are identical. Actually, the modulated carriers, including Doppler

* These experiments were performed under Contract NASW-110 for the National Aeronautics and Space Administration.

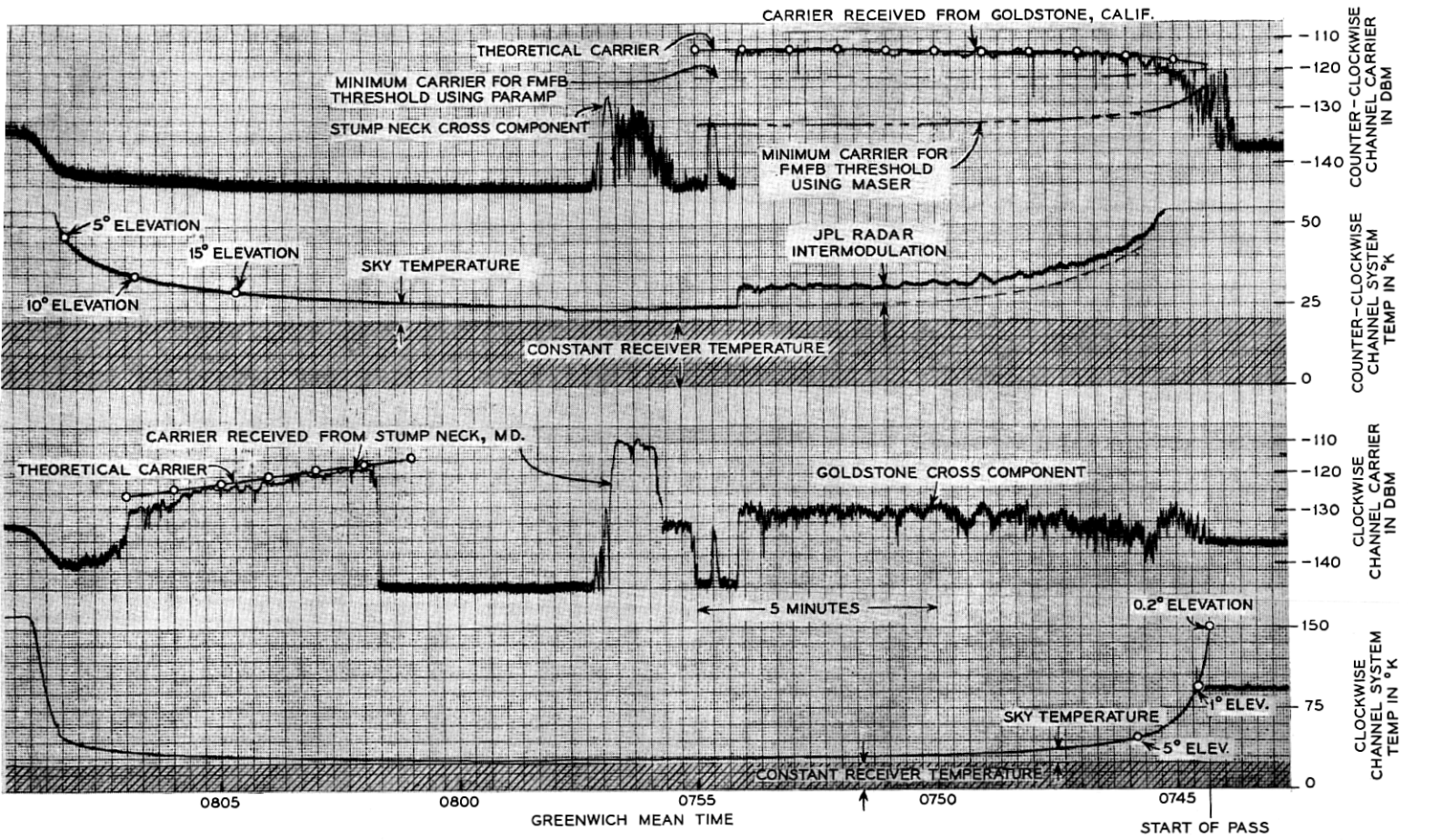

Fig. 4 — Typical receiver recordings (for Pass 60, August 17, 1960).

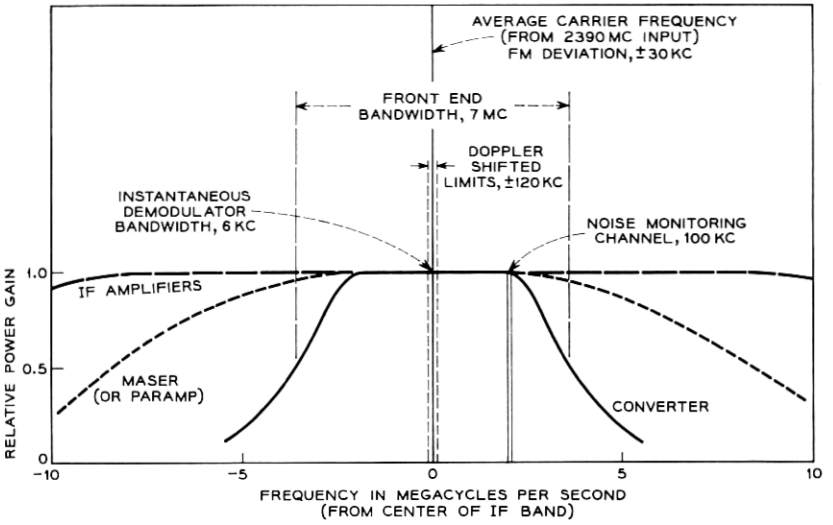

Fig. 5 — Receiver bandwidths.

shifts, occupy only a small portion of the "front-end" bandwidth, as shown in the center of Fig. 5; this permits the use of a simple circuit that can continuously monitor the system temperature while carriers are also being received. Assuming constant gain it can be shown that the output noise from any slice of the "front-end" bandwidth is proportional to the system temperature. In order to eliminate carrier interference, the noise temperature monitoring channel was chosen as far as practical from the carrier frequency, as is also shown in Fig. 5.

A second output of each IF transmission line is accordingly connected to a *system temperature monitor*, where the required selectivity is achieved with a very narrow-band IF amplifier. By following this with a precision square-law detector, a dc output voltage is obtained which is proportional to the system temperature. To calibrate this output voltage a known amount of excess noise from a standard noise lamp is added to the input waveguide via the 18-db directional couplers shown in Fig. 3. The resulting calibrated voltages, which indicate system temperature, are also shown in Fig. 4, where they are labeled "counter-clockwise channel system temperature" (second from top) and "clockwise channel system temperature" (bottom recording).

The *frequency counter* output was used to tune the FM demodulators in the presence of large Doppler shifts, and the *2B noise set* was used to verify the quality of the satellite system voice circuits.

Thus the useful receiver outputs are two audio circuits, one for each sense of circular polarization, and a set of four calibrated voltage records, which represent the received carrier powers and noise temperatues for each polarization. These recordings, also seen in Figs. 10 through 21 of Ref. 4, show how the west-to-east satellite system was operating at all times.

III. SYSTEM NOISE TEMPERATURE

The sky, antenna, waveguide, maser, and converter all made significant contributions to the system noise temperature. This section shows by the use of measurements, calculations, or reasonable estimates how much temperature was added by each of these sources. The sum of these temperatures is found to be in fair agreement with measurements of the over-all system temperature. Details of the over-all system measurements are given in Appendix B.

3.1 *Sky*

Since the background sky temperature, which varies with the antenna elevation angle, is always observed by a satellite-tracking antenna, it is necessary to include it as a part of the system noise temperature. As shown in the lower curve in Fig. 2, the sky temperature contribution (measured as shown in Appendix C) is only 2.3°K at the zenith but increases to 25°K when the antenna is lowered to a five-degree elevation. Thus, about 23°K must be added to the system temperature at the zenith in order to design a system which will work down to this elevation. Closer than this to the horizon the sky temperature increases even more rapidly, and as a result it becomes progressively more difficult to provide a system for satellite communications. Fortunately the higher temperatures are only present for a small portion of a pass as shown by the typical system temperature recordings of Fig. 4. Although communications cannot typically be maintained close to the horizon, this time can be well spent in acquiring the satellite and making preliminary carrier-level measurements.

Although there are additional isolated sources of sky temperature, they are not usually encountered during a satellite pass because they are few and far between. The sun, however, which has a temperature of 40,000°K at 3 kmc, can add about 4000°K via the main beam of the antenna. The added temperature is less than the sun temperature because the antenna beamwidth, about 1.25 degrees in this case, is greater than the angle subtended by the sun, which is 0.5 degree. The sun was also observed to add

from 5 to 20°K via various side lobes. Using the main beam, the hottest radio star, Cassiopeia A, was found to add 14.3°K, the moon about 16°K, and the center of the galaxy 4.5°K. Incidentally for a more uniform sky temperature reference, the antenna should be pointed about 14 degrees south of the zenith, a region traversed by fewer and cooler radio stars.

3.2 *Antenna*

The tracking horn antenna is described in a companion paper by Crawford, Hogg, and Hunt.[5] It is similar to those used for microwave radio relay; its main advantage for a low-noise system is that the exceedingly low back and far side lobes* reduce interference, and are estimated to add only 2 ± 1°K to the system temperature. This estimate is based on the temperature "not otherwise accounted for" in a previous experiment;[3] it is somewhat larger than the calculated temperature expected from back lobes measured on a similar antenna.

A second advantage is that a long waveguide run, which adds to the system temperature, is not required. A third advantage is that the way this antenna can be mounted[5] makes it convenient to provide a shielded laboratory for the preamplifiers and associated receiving equipment.

3.3 *Waveguide*

The purpose of the waveguide assembly is to transmit the received circularly polarized energy from the antenna to the preamplifiers with the minimum amount of added noise. The waveguide assembly is shown in Fig. 3 and its general operation was described in Section II. Since each 0.1 db of insertion loss adds about 7°K to the system temperature, it was well worth while to minimize waveguide losses. Broadband components are used throughout in order to minimize the use of lossy tuning devices. The possibilities of significant resonance losses were eliminated by adjusting each component to have a return loss of 35 db or greater over a 100-mc bandwidth. In addition, all parts were made as short as practical. A summary of the loss of each waveguide component is given at the end of this subsection in terms of the equivalent increase in system temperature or "loss temperature." The particular source of this temperature, i.e., whether based on a measurement, calculation, or an

* Although the side lobes near the main beam are normal in size, they are usually pointed toward the cold sky, and therefore do not add much to system temperature. This is confirmed in Fig. 2 by the close agreement between the measured and theoretical sky temperatures. As can be seen the agreement is good from the zenith down to an elevation angle of only $1\frac{1}{2}$ degrees.

estimation of the insertion loss, is also indicated. The unique features of the waveguide assembly are discussed below.

3.3.1 *Rotating Joint*

The most important practical aspect of the waveguide assembly is the rotating joint, which allows the antenna to rotate in elevation while the rest of the receiver is connected solidly to the floor of the antenna cab. This, of course, eliminated the need for designing equipment to swing $\pm 45°$ with the antenna elevation.

A cross section of the rotating joint is shown in Fig. 6. The purpose of the multiple chokes is to reduce the insertion loss and to drastically reduce leakage from the antenna cab calibration equipment into the receiver front end. Assuming a high (free-space) impedance at the outer edge, all lengths were adjusted to give the minimum impedance at the inner surface of the waveguide. L_1, L_3, and L_5 were found from Schelkunoff's analysis[6] of cylindrical cavity resonators. As shown by Mum-

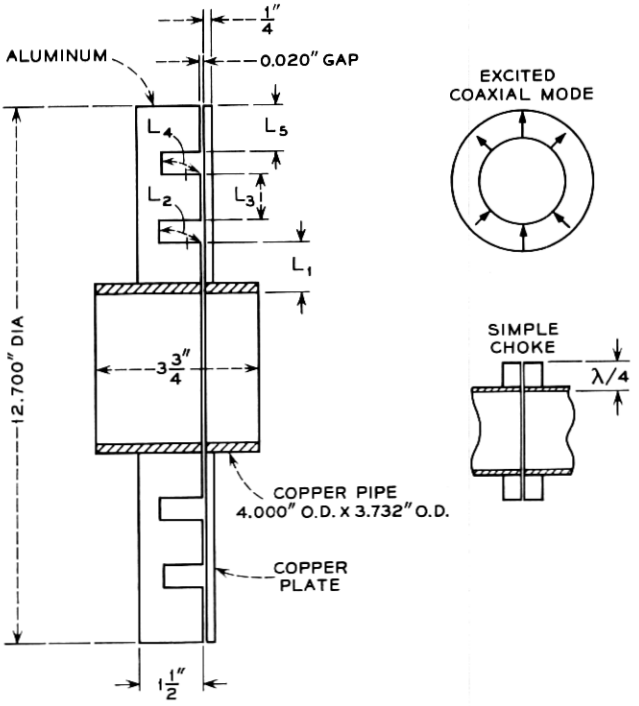

Fig. 6 — Rotating joint.

ford,[7] the desired lengths are somewhat shorter than a quarter wavelength due to the greater capacitive loading at the smaller radii. L_2 and L_4 were adjusted to resonate with L_1 and L_3 assuming excitation of the TE_{01} coaxial mode,[6] which is also shown in Fig. 6.

The total measured loss temperature of the rotating joint assembly is only 0.14 ± 0.02°K, and the gap itself accounts for only about 0.05°K of this. For comparison purposes, the loss temperature of a simple choke, also shown in Fig. 6, is about 1°K using dominant-mode waveguide, and about 0.4°K using oversize waveguide which has a diameter of 1.4 wavelengths. It was also noted that the nominal 20-mil gap is adequate to allow for residual mechanical distortions of the supporting structure and that the loss temperature increased about 15 per cent due to 15-mil offsets of the rotating portion of the joint. These offsets are due to the slightly eccentric rotation of the antenna throat.

3.3.2 *Finline*

The waveguide assembly also acts as a circular polarization filter in that it separates the two senses of incident circular polarization. This action can be explained as follows. Any circularly polarized wave can be thought of as two linear waves at right angles in space and displaced 90° in time phase from each other, as shown at the top of Fig. 7. An observer at "A" would see a wave that rotates in the counter-clockwise direction. If wave #1 is retarded a quarter-wavelength or 90° with finline (or other) loading, a vertically polarized wave will result. Similarly, if #1 had been lagging #2, instead of leading, the observer at "A" would have seen a clockwise rotation. If #1 is now retarded 90° by the same finline, #2 and #1′ will be lined up. The result is a horizontally polarized wave. Thus the counter-clockwise wave is transformed to vertical, and the clockwise wave to horizontal linear polarization by the 90° retardation of one linear component. This finline $\Delta 90°$ component was designed with only a modest fin penetration, as shown at the bottom of Fig. 7, in order to keep the insertion loss low and to reduce the residual mismatch. The required match was achieved by dividing each fin taper length into three $\lambda_g/4$ segments and adjusting the slopes of these three consecutive segments to be in the ratio of $1:\sqrt{2}:1$ (this ratio was found empirically to give the best broadband match). The measured relative phase shift was 90 ± 1 degrees at 2390 mc. The power coupled from one channel to the other, due to the ± 1 degree tolerance, is down at least 40 db.

3.3.3 *Polarization Coupler*

The pertinent details are shown in Fig. 8. Because of the unique triangular plates the return loss of the "straight-through" polarization was

greater than 40 db over many octaves. There is some power cross coupled from one polarization to the other because of small mechanical assymmetries, but this is also down at least 40 db.

The polarization filter consists of the finline in combination with the adjacent polarization coupler oriented as shown in Fig. 3. After allowing for arbitrary phasing of the above couplings, and since the rotating joint and antenna throat are fairly symmetrical, it appears that the total power that can be coupled from one channel to the other (via the waveguide) must be down at least 34 db.

3.3.4 *Antenna Throat*

The cross sections of this taper were varied smoothly to give a "raised cosine" distribution of reflection coefficient per unit of waveguide wavelength. For the slopes of this antenna feed horn about three wavelengths

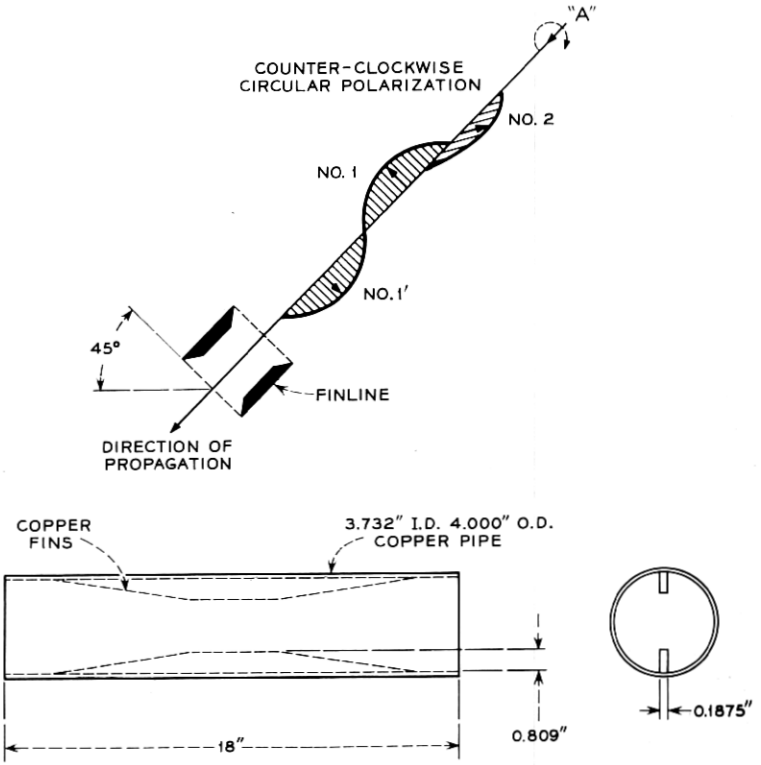

Fig. 7 — Finline 90° section.

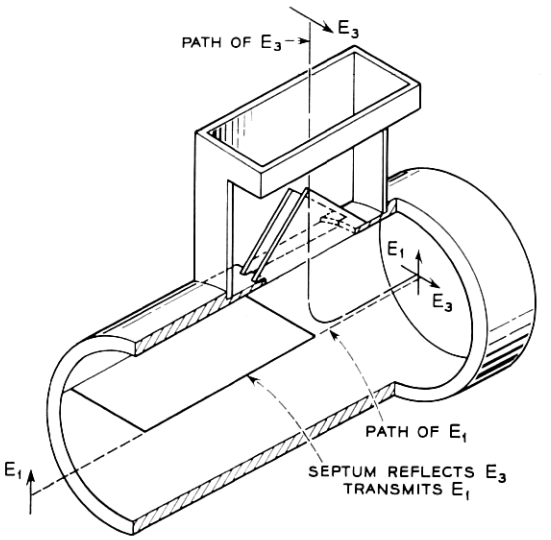

Fig. 8 — Polarization coupler.

are required to go from the constant impedance of free space to that of the dominant mode waveguide (a ratio of 1.7 to 1). Bolinder[8] shows that the theoretical return loss for this length is a respectable 67 db. Therefore this well-matched electroformed throat turned out to have an excess length, i.e., beyond the apex of the antenna throat, of only one-half wavelength. Assuming an increased loss factor of 1.25 for surface roughness for electroformed copper,[9] the temperature contribution of this component was calculated to be $0.33 \pm 0.05°K$.

3.3.5 *Waveguide-to-Coaxial Transducer*

Because of its near-minimum attenuation constant, a 72-ohm characteristic impedance was chosen for the maser input coaxial line. The coaxial probe of this transducer was otherwise conventional, but it had to be carefully adjusted in length and location to achieve the lowest possible insertion loss. Another feature of this component is a new location for the maser vacuum seal. It was moved from a cold location in the coaxial line to the much warmer waveguide connecting flange in order to prevent increased loss from water condensation. The seal itself is an 11-mil sheet of Mylar cemented in a countersunk flange with a special adhesive. The outer wall of the coaxial line was connected to the transducer with a commercial flare fitting. This provided an excellent vacuum connection

when used with a thin soft-copper flared-washer seal and made it possible to disconnect the maser quickly for an emergency switch to the parametric amplifier.

3.3.6 *Directional Coupler*

The measured coupling of the conventional cross-guide coupler is 18.15 ± 0.15 db. It can be shown that the loss temperature, due to the insertion loss, can be calculated from

$$T°\mathrm{K} = \frac{290}{\log^{-1} \frac{\mathrm{db}_{\mathrm{coupling}}}{10}}.$$

The loss temperature in this case is 4.45 ± 0.15°K. When a parametric amplifier is used, an 18-db coupling is needed to add sufficient noise from an argon lamp for a system temperature measurement. Using a maser the coupling could be reduced to 27 db and the corresponding loss temperature would then be a less objectionable 0.7°K. For the Echo experiments it was decided to retain the 18 db-couplers in order to allow a faster switch to the standby parametric amplifiers.

The wall loss adds about 0.20 ± 0.02°K for a total loss temperature of 4.65 ± 0.17°K.

3.3.7 *Summary*

The loss temperatures of many of the waveguide parts were calculated using the measured attenuation constants of the round and rectangular waveguides. These calculations include estimates, when necessary, for the somewhat higher insertion losses due to "greater than dominant mode" wall current densities. The loss temperatures of all the waveguide parts are summarized in Table I.

TABLE I — WAVEGUIDE SOURCES OF SYSTEM TEMPERATURE

Source	Counter-Clockwise Channel	Clockwise Channel	
Throat	0.33 ± 0.05°K	0.33 ± 0.05°K	calculated
Rotating joint	0.14 ± 0.02°K	0.14 ± 0.02°K	measured
Finline	0.46 ± 0.06°K	0.46 ± 0.06°K	calculated
Polarization coupler (bend)	0.48 ± 0.05°K	0.48 ± 0.05°K	measured
Polarization coupler (straight)	—	0.23 ± 0.04°K	calculated
Rectangular waveguide	0.19 ± 0.02°K	—	calculated
Directional couplers	4.65 ± 0.17°K	4.65 ± 0.17°K	calculated
E-plane bend	0.25 ± 0.03°K	—	calculated
H-plane bend	—	0.27 ± 0.03°K	measured
Waveguide-to-coaxial transducer	0.50 ± 0.25°K	0.50 ± 0.25°K	measured
Predicted total	7.00 ± 0.65°K	7.06 ± 0.67°K	

The total loss temperature of the waveguide could be reduced about 0.5°K by using higher conductivity copper (which is commercially available) in place of red brass (which was used for the rectangular parts) and impure copper (which was used for the round parts).

3.4 *Maser*

This low-noise preamplifier assembly is described in a companion paper by DeGrasse, Kostelnick, and Scovil.[10] It had the ability to amplify the incoming carrier and noise more than 36 db without adding more than 8°K to the system temperature. The large gain was required in order to reduce greatly the system temperature contribution from the following converter. The gain was also very stable, an important factor in keeping the receiving system properly calibrated. The variation during a half-hour period, from the initial input carrier level calibration before a satellite pass until the recheck after the pass, was typically only a few tenths of a decibel.

3.5 *Converter*

Since the converter system temperature contribution (referred to the amplifier input) is the converter temperature reduced by the net gain from the input, a low noise figure was required. Since the maser saturation threshold occurs at an output level of −40 dbm, low leakage from the local oscillator was also desirable. To meet these requirements a balanced converter using 1N263 diodes was designed by R. H. Turrin. It had a noise figure of 7.5 db (1300°K) and local oscillator leakage power on the order of −20 dbm. The leakage power was further reduced to −47 dbm with a coaxial isolator. Since the additional loss between the maser and converter was 2.3 db (1.35 db for interconnecting coax, 0.75 db for the isolator, and 0.2 db for a monitoring directional coupler) and the maser gain was 36.3 db, the net gain from the input was reduced to 34 db. The converter system temperature contribution was therefore calculated to be 0.6 ± 0.15°K. The limits are due mainly to measured day-to-day changes of the maser gain.

3.6 *Total System Temperature*

A rough idea of the total system temperature was found by adding together the contributions of all of the known sources, as shown in Table II.

The total system temperature was also measured by using the noise-lamp technique which is discussed in Appendix B. Using this method

TABLE II — SOURCES OF SYSTEM TEMPERATURE

Source	Temperature
Sky (at zenith)	2.30 ± 0.20°K
Horn antenna	2.00 ± 1.00°K
Waveguide (counter-clockwise channel)	7.00 ± 0.65°K
Maser assembly	7.00 ± 1.00°K
Converter	0.60 ± 0.15°K
Predicted total system temperature	18.90 ± 3.00°K

the temperature was found to vary a few degrees from day to day, but the lowest temperature was consistently 22.2 ± 2.2°K. By realistically assuming that all sources were then contributing their fair share (as is also tacitly assumed in Table II) it is possible to improve the over-all accuracy. The actual system temperature must be in the overlap region of the measured results and the total results of Table II, namely between 20 and 21.9°K. The most likely minimum system temperature was therefore

$$T_{\text{system}} = 21 \pm 1°\text{K}.*$$

The inference from this result is that the "+" temperature possibilities of Table II must predominate.

3.7 *Parametric Amplifier*

This fairly low noise "standby" preamplifier is described in a companion paper by Kibler.[11] The receiving system was designed so that the "paramp" could be switched into the system, tuned, and calibrated in about 15 minutes. The chief effect of using it in place of the maser was to increase the minimum system temperature to 290°K. The resulting temperatures for all angles of antenna beam elevation are shown by the upper curve in Fig. 2. The paramp gain usually decreased about a decibel during a pass, and this turned out to be a limiting factor in the received carrier calibration accuracy.

IV. FM DEMODULATOR AGC CHARACTERISTICS

The FM features of the demodulator are discussed by Ruthroff.[2] The purpose of this section is to show how the AGC voltage features were exploited in order to obtain accurate recordings of the 2390-mc received carrier power.

A simplified block diagram of the FM demodulator (Fig. 3 of Ref. 2) shows that there are two feedback loops, one for FM, and the other for

* 17.25 ± 1°K without the paramp standby provision, i.e., with a 27 db waveguide directional coupler in place of the 18 db coupler.

AGC. The purpose of the FM loop is to make the VCO frequency track the FM deviations of the input carrier. The primary purpose of the AGC loop is to keep the 1.2-mc carrier amplitude at the limiter input fairly constant over a wide range of input power. The secondary purpose is to calibrate the AGC voltage as a function of known 2390-mc input carriers and, conversely, deduce the input levels from AGC voltages generated by the actual received carriers.

Since the AGC voltage is derived from the amplitude of the carrier and/or AM noise in the path common to both feedback loops, it is also a function of the FM demodulation process. It turns out that the maximum AGC voltage is always obtained where the FM demodulator is "tuned" by properly adjusting the VCO frequency. For strong carriers it was found that the audio circuit quality was always improved by maximizing the AGC voltage; and for weak carriers, i.e., those below the FM threshold, it was found that erratic AGC voltages could be readily maximized by using audio quieting as a tuning aid.

A practical feature of the demodulator was that all tuning was readily accomplished with a single control. This made it possible to calibrate just before and after each pass to decrease long-term drift errors. Aided by the VCO frequency counter, this also made it possible to acquire readily and track accurately the received carriers despite Doppler shifts of ± 90 kc. The feeling from this experiment was that automatic frequency tracking could and should be provided for future satellite receivers.

A typical FM demodulator AGC characteristic is shown in the right-hand curve of Fig. 9. The known 2390-mc carriers were inserted via the waveguide couplers after the input noise was minimized by pointing the antenna toward the zenith. For reference, the curve on the left in Fig. 9 is an AGC characteristic which was obtained by using equivalent 70-mc carriers that were essentially noise-free. As can be seen, the net gain from the "front end" was adjusted to utilize the region of highest AGC voltage. This placed the AGC "voltage range of interest" in the most linear portion as shown on the right, and this also gave the most nearly constant amplitude at the limiter input. The 2390-mc AGC characteristic is identical to the noise-free reference for carrier levels well above the threshold. As the 2390-mc carrier is decreased below the threshold the AGC characteristics begin to diverge. The reason for this is the FM loop loses control, which intermittently detunes the receiver. For a correct average VCO tuning and an unmodulated received carrier the AM noise increases, and this in turn increases* the AGC from the "noise-free" case in a known reproducible way, as shown by the right-hand curve in Fig. 9. As the

* Modulated carriers will decrease the AGC voltage somewhat.

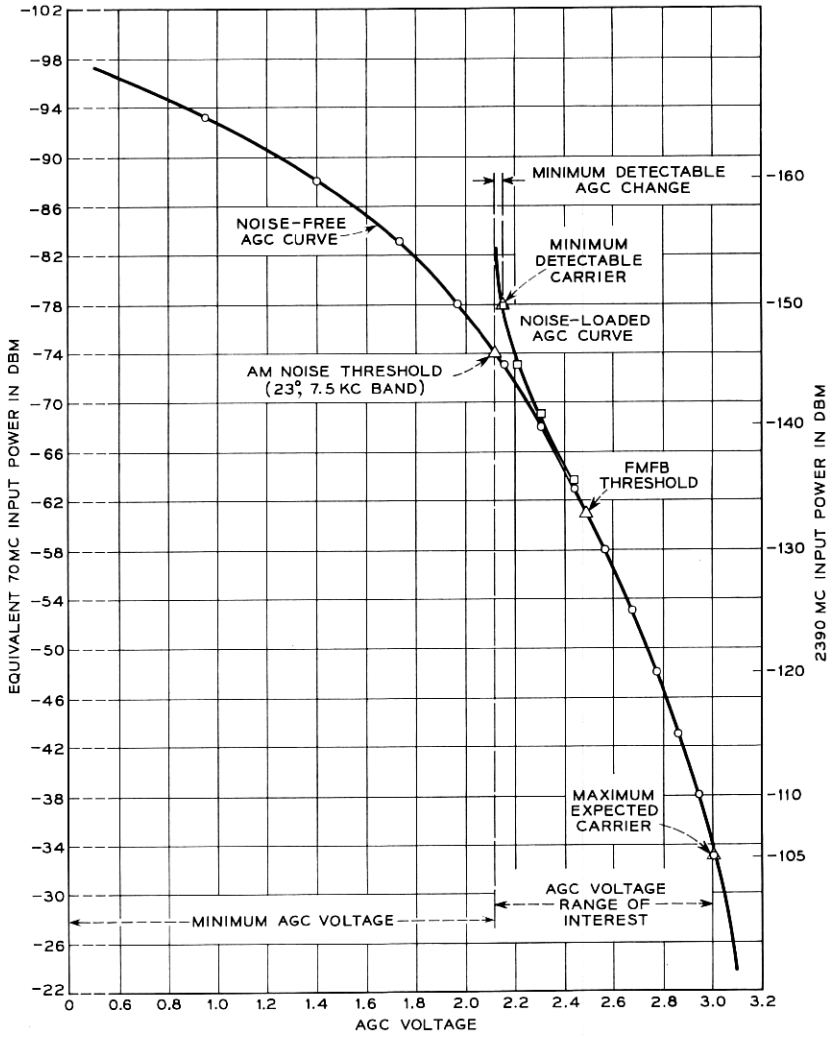

Fig. 9 — FMFB demodulator AGC characteristics.

2390-mc input is decreased well below the threshold a minimum AGC voltage is reached as shown by the sharp vertical rise of the right-hand curve in Fig. 9. This limit is due to noise power from the front end; it will now be calculated. Since the FM feedback is ineffective at these levels the demodulator acts like an AM detector. The noise bandwidth of the demodulator AGC circuit is given by the bandwidth when the FM loop

is open[2] and is only 7.5 kc. For a 23°K system temperature the limiting noise power is −146 dbm. As in other AM systems, a somewhat smaller carrier will cause an observable change in the AGC voltage and, as shown in Fig. 9, the minimum detectable carrier for this demodulator was −150 dbm. The significance of this was that the carrier could be detected and measured down to the horizon and the cross component could be readily monitored during most of each pass.

The AGC "voltage range of interest" of Fig. 9 was attenuated somewhat and back-biased in order to use the total recorder chart area as shown by the top recording of Fig. 4. The 2390-mc input carrier power calibrations are shown on the right-hand edge. The over-all calibration accuracy was limited mainly by uncertainties of the input carrier powers, and is estimated to be within 0.5 db of nominal. The time constant of the AGC circuit was about 0.02 second; since the typical fades were much slower, none of the fading rates shown on any of the AGC recordings was limited by the recording equipment.

In addition to the received carrier measurements some noise measurements were made with the over-all receiving system in order to verify the audio FM demodulator characteristics. Since the threshold carrier-to-noise power (referred to a 6-kc band) is 14 db and the average temperature at the zenith, 23°K, the minimum threshold carrier power was calculated to be −133 dbm. The actual threshold carrier was found by noting the minimum calibration power required to avoid "popping" in the audio circuit when the antenna was pointed toward the zenith. This turned out to be −133 dbm, as expected.

The quality of the audio circuit was verified as follows. Shortly *before* a pass a 70-mc FM test oscillator was temporarily connected to the demodulator input. The carrier level was set equal to that anticipated from the satellite system. The FM (sine wave) deviation was set at the maximum allowed by the demodulator, and the corresponding maximum audio power was measured at the output with a 2B noise set. The audio output noise from the received unmodulated carrier was then measured *during* the pass. These results were combined to give a reasonable indication of the signal-to-noise ratio. The carrier of the corresponding carrier-to-noise ratio was found from the calibrated AGC voltages, and the noise power (referred to a 6-kc band) was calculated from the observed system temperature. The resulting signal-to-noise ratio versus carrier-to-noise ratio was plotted and found in good agreement with previous laboratory results, as well as with the results predicted from FM theory, all shown in Fig. 27 of Ref. 4.

The main characteristics of the receiver are summarized in Table III.

TABLE III — OVER-ALL RECEIVER CHARACTERISTICS

Nominal frequency	2390 mc
Two channels	One for each sense of circular polarization
RF cross coupling (between channels)	−34 db
Audio bandwidth (each channel)	0.2 to 3 kc
Maximum FM deviation	±30 kc
Minimum system temperature	21 ± 1°K*
Minimum threshold carrier power	−133 dbm
Minimum detectable carrier power	−150 dbm
Carrier calibration range	−110 dbm to −150 dbm
Time constant of carrier recordings	0.02 second
Carrier calibration accuracy	From ±0.5 db above threshold to ±2 db well below threshold

* 17.25 ± 1°K without a paramp standby provision.

V. EXPERIMENTAL RESULTS

The main experimental results, which include complete data of the west-to-east satellite systems, are given by the four-channel pen recordings shown in Figs. 10 through 21 of Ref. 4. Two high-quality voice circuits, with signal-to-noise ratios greater than 36 db, were also available from the receiver whenever the resulting ratio of received carrier-to-noise power (referred to a 6-kc band) exceeded 14 db. These experimental results are shown in Fig. 27 of Ref. 4.

A locus of the minimum carrier level required during a typical pass (for the critical 14-db carrier-to-noise ratio) is shown in the top recording of Fig. 4. For convenience, this is superimposed on a recording of a carrier received from Goldstone under good tracking conditions. The minimum carrier level required using a paramp instead of a maser is also shown. These plots verified the fact that a good voice circuit could be achieved using the paramp under modest carrier fading conditions (which are shown) and that the fading margin for a good voice circuit using the maser was about 16 db over most of a pass. (This is significant, since the consistent maximum fading due to the balloon* turned out to be only 10 db.)

After accounting for some known transmitter, refraction, and tracking errors, the calibrated carrier level recordings verified that the entire communication system was working properly, and that the path losses were characterized by the propagation laws of free space. The recordings also measured the random variations that occurred during every operational pass and the random decreases in average level that occurred from pass to pass.

* Shown in Pass 1086, after 0944 GMT (Fig. 20 of Ref. 4).

Certain observed characteristics of the carrier level recordings were also used to identify some otherwise unknown transmitter tracking errors. The key characteristics were (a) a much more jagged than normal carrier level recording, especially in conjunction with a lower than normal average level;* (b) an anomalous increase in carrier level adjacent to a gross pointing error;† and (c) a period of decreased main carrier level, with simultaneous increase in the average cross-component level.‡ These additional clues made it possible to eliminate some questionable data in order to evaluate more accurately the reflection characteristics of the balloon.

The recorded system temperatures verified that the background sky temperature varied as anticipated, and that the isolated sources of large sky temperature were seldom encountered. The temperature recordings also showed that other sources, such as lightning, clouds, nearby radars, and radio stars occasionally added only a few degrees to the system temperature.

VI. ACKNOWLEDGMENTS

There were several people, in addition to those already mentioned, who made significant contributions to this receiver. The complex assembly and testing, in particular, could not have been accomplished on schedule without the timely and generous aid of W. W. Snell, who rendered alert, critical assistance, and H. A. Anderson, who ingeniously solved many of the complicated installation problems. Other timely aid was provided by H. E. Keller, who tuned the waveguide parts, F. A. Dunn, who constructed and tested the very-narrow-band IF amplifiers, R. A. Semplak, who provided the crystal-controlled local oscillator, R. H. Turrin, who designed the crystal converters and tuned the antenna slip-ring assembly, and W. E. Legg, who assembled the RF generator needed to "pump" the maser. The precision square-law detectors (with large output voltages), the precision system temperature measurements (needed to determine the sky temperature), and the automatic nitrogen transfer system are all due to W. W. Snell. Aid in operating the receiver was provided by E. L. Frantsvog (helium transfers), R. A. Desmond (calibration), and W. F. Bodtmann (FM demodulator tuning). After the Echo I experiments were concluded, the waveguide losses were precisely measured by G. S. Axeling.

Although this equipment was designed by the Bell System as part of

* Shown in Pass 1086, prior to 0944 GMT (Fig. 20 of Ref. 4).
† See Pass 229 at 0453:30 GMT (Fig. 15 of Ref. 4).
‡ See Pass 60 at 0756:50 GMT (Fig. 4 of this paper).

its research and development program, it was operated in connection with Project Echo under Contract NASW-110 for the National Aeronautics and Space Administration.

APPENDIX A

Front-End Tuning

In order to maintain the low inherent system temperature and calibrate the receiver before and after each satellite pass, a fast, easy-to-use measuring system was required. Such a system was interconnected to both channels of the receiver; the connections to a single channel are shown in Fig. 10. Front-end RF test signals were generated in the antenna cab and inserted into the receiver via an 18-db waveguide directional coupler. The IF results were then readily monitored and/or measured via a permanently installed IF coupling network.

All required signal levels were achieved by attenuating a known reference power with coaxial attenuators, as shown in the lower left of Fig. 10. Since the calibrated input carriers were as low as −150 dbm, shielding precautions were required to reduce RF leakage from the test equipment to the input waveguide. Some highly effective features were the multiple

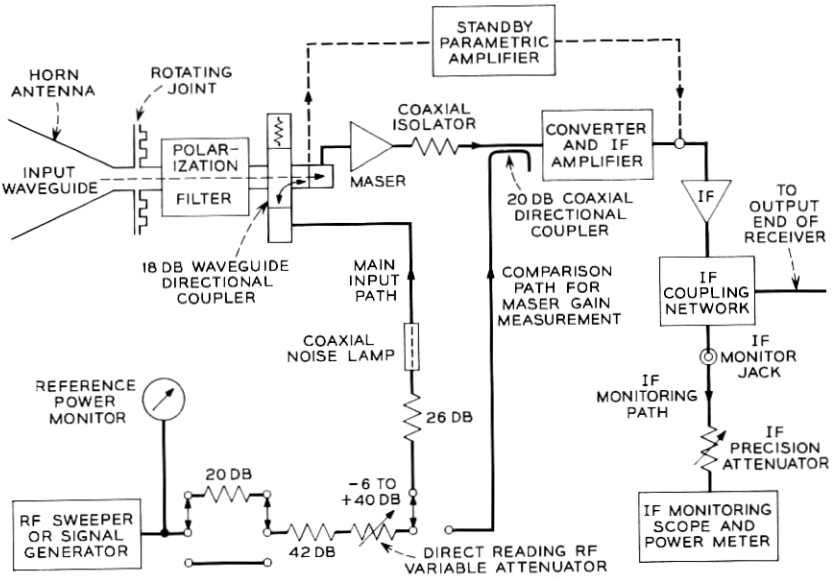

Fig. 10 — Front-end measuring system.

chokes used around the waveguide rotating joint and the well-shielded General Radio connectors used for coaxial attenuator switching. The attenuator values were selected to prevent (after proper switching) erroneous results due to saturation effects or poor carrier-to-noise ratios. The selected values also allowed the use of a direct-reading General Radio RF attenuator for the entire input carrier calibration range.

The first tuning step was to optimize the bandpass characteristic of the maser or the paramp, using a swept signal well above the noise. The maser gain was then found by comparing the known input carrier power with that required when it was inserted after the maser (via the permanently installed 20 db coaxial directional coupler). The monitored IF power was held constant for this measurement. Alternatively, the paramp gain was found by inserting a known input carrier and comparing this to the 70-mc power at the IF monitoring jack. After achieving the normal gain and frequency range the system temperature was checked as shown in Appendix B. The final step was to furnish known input carriers to calibrate the AGC voltages (about 10 minutes before each pass). As again can be seen in Fig. 10, this was done by simply adjusting the direct-reading RF attenuator when the fixed attenuators were connected as shown.

APPENDIX B

System Temperature Measurements

After the antenna had been pointed toward the zenith, data for the system temperature were found by coupling excess noise from an argon noise lamp into the input waveguide as shown in Fig. 10 and then measuring the increase in IF output power. The system temperature was then calculated from

$$T_{\text{system}} = \frac{T_H L_{\text{coax}} L_{\text{coupler}}}{Y - 1},$$

where T_H is the excess noise at the output terminal of the coaxial noise lamp, L_{coax} is the insertion loss between the noise lamp and the directional coupler, L_{coupler} is the coupling loss of the waveguide directional coupler, and Y is the ratio of lamp "on" to lamp "off" power at the IF monitor jack. T_H was calculated[12] using the measured[3] electron temperature of a similar argon lamp (10,500 ± 265°K at 6 kmc), and the measured insertion losses (15.5 db "on" and 2.4 db "off") for this particular coaxial noise lamp mount. The result was $T_H = 8360 \pm 225$°K. The measured insertion loss of the coaxial line was 1.31 db and the measured coupling

of the directional coupler was 18.15 ± 0.15 db. Therefore the total excess temperature coupled into the waveguide, T_{coupled}, was 94.6 ± 6°K, and

$$T_{\text{system}} = \left(\frac{94.6 \pm 6}{Y - 1}\right) \text{°K}.$$

Using a paramp, the observed values of Y varied from 1.30 to 1.35. The corresponding paramp system temperatures are 270 and 315°K. Using a maser, Y was typically about 5 and therefore the maser system temperature was about 23°K. A 27-db coupler could have been used instead of the 18-db coupler to reduce Y to a still acceptable value of 1.65. This would also have reduced the system temperature 3.75°K. For the paramp, however, Y would then have been too small for a meaningful measurement. The 18-db couplers were therefore retained in service to provide a standby measuring technique for the paramp system temperature. The resulting system temperatures for other antenna beam elevations are shown in Fig. 2.

APPENDIX C

Sky Temperature

Since the sky temperature seen by a narrow beam antenna is proportional to the length of antenna beam passing through each layer of atmosphere, the sky temperature at the zenith, whatever its value, will approximately double when the antenna beam is lowered to an elevation of 30 degrees. It will redouble at 14.5 degrees, quadruple at 7.2 degrees, etc., as given by

$$T_{\text{sky}} \text{ at } \theta \cong \frac{T_{\text{sky}} \text{ at } \theta_z}{\sin \theta} \qquad \theta > 5°, \tag{1}$$

where θ is the elevation of the antenna beam above the horizon and θ_z is an elevation of 90°. It turns out that only a narrow range of sky temperatures, when doubled, redoubled, etc. (and added to a constant), will match the observed maser system temperatures. Following this restraining principle, it can be shown that the sky temperature at the zenith can be determined from the maser system temperatures and the theoretical ratio, N, of T_{sky} at θ to T_{sky} at θ_z. This result is given by

$$T_{\text{sky}} \text{ at } \theta_z = \frac{T_{\text{system}} \text{ at } \theta - T_{\text{system}} \text{ at } \theta_z}{N - 1}, \tag{2}$$

where N, derived from (1), is given by

$$N = \frac{T_{\text{sky}} \text{ at } \theta}{T_{\text{sky}} \text{ at } \theta_z} \cong \frac{1}{\sin \theta}. \tag{3}$$

For improved accuracy, more exact values of N which take into account the curvature of the earth's atmosphere should be used (these ratios can be found from the results of a theoretical derivation of sky temperature[13]); random experimental limits should be allowed for; and the required use of zenith system data should be eliminated. A more general form of (2) was therefore derived which allows these advantages:

$$T_{\text{sky}} \text{ at } \theta_z = \frac{\left(\frac{T_{\max} \text{ at } \theta + T_{\min} \text{ at } \theta}{2}\right) - \left(\frac{T_{\max} \text{ at } \theta_0 + {}_{\min}T \text{ at } \theta_0}{2}\right)}{N_\theta - N_{\theta_0}}, \tag{4}$$

where $T_{\max}$ and $T_{\min}$ are the respective temperature limits (after allowing for random experimental errors) for two elevations, θ and θ_0; and N_θ and N_{θ_0} are the theoretical sky temperature ratios, defined in (3), for these two elevations. For greatest accuracy, many different combinations of θ_0 and θ (chosen to be widely separated) must be used and great care must be exercised to allow for random increases in system temperature due to the antenna side lobes.

It can also be shown that the limits of the sky temperature are given by

$$\Delta T_{\text{sky}} \text{ at } \theta_z = \pm \frac{\left(\frac{T_{\max} \text{ at } \theta - T_{\min} \text{ at } \theta}{2}\right) + \left(\frac{T_{\max} \text{ at } \theta_0 - T_{\min} \text{ at } \theta_0}{2}\right)}{N_\theta - N_{\theta_0}}.$$

By selecting measured maser system temperatures from Fig. 2 for many pairs of elevation angles down to 5°, the sky temperature at the zenith was found to be

$$T_{\text{sky}} = 2.30 \pm 0.2°\text{K}.$$

This was in good agreement with the theory, which had predicted a value of 2.4°K.

APPENDIX D

Liquid Nitrogen

The outer dewar of the maser had to be kept cold with liquid nitrogen and, due to "boil-off," the liquid in the dewar had to be replenished

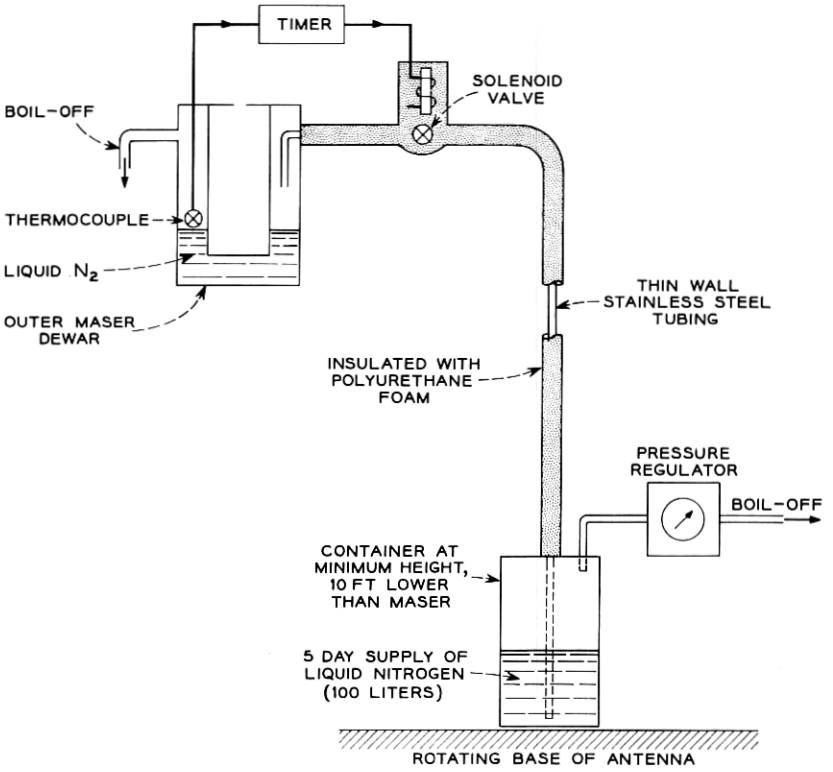

Fig. 11 — Automatic liquid nitrogen transfer system.

every 12 hours. Fig. 11 shows how batches of liquid were automatically supplied for periods of five days. Since it was too heavy and bulky to go into the antenna cab, the 100-liter supply container was located on the rotating base of the antenna. The boil-off losses of the resulting long transfer line were kept within reason by using thin wall stainless steel tubing surrounded by an insulating foam.

The sensing device of the system was a thermocouple furnished in the outer maser dewar which sent a signal to the timer when liquid was required. The timer kept the solenoid valve open just long enough to fill the dewar. The liquid was pumped through the open solenoid valve at a predictable rate by the storage container "back pressure." This was stabilized by the pressure regulator, which could also adjust the back pressure for different flow rates.

Although preliminary cooling of the line (and valve) during the trans-

fer process boiled off some nitrogen, changing of output flow from warm to cold gas and then increasing quantities of liquid greatly reduced the thermal shock on the dewar. This system, designed and built by W. W. Snell, is highly recommended for automatic nitrogen servicing.

APPENDIX E

Liquid Helium

In order to operate the maser, the inner maser dewar had to be cooled with liquid helium.

Because liquid helium has an extremely low temperature and a low specific heat, special vacuum-insulated storage and handling facilities were required to prevent excessive "boil-off" losses. The resulting storage containers were therefore quite heavy and the liquid had to be "transferred" (from storage to another dewar) in batches via vacuum-insulated transfer lines.

For daily maser operations large quantities of liquid were required, and these could not be supplied locally. The necessary amounts were accordingly shuttled every fourth day from Tonawanda, New York, in two special 100-liter containers. This type of "super-insulated" container was selected because it could conveniently supply the maser for four days from a platform on the rotating base of the antenna. This eliminated the need for daily heavy lifting, and indeed all lifting, since the platform could be easily reached by truck. Another convenient feature of this container was that liquid nitrogen servicing was not required. As a result, the container was relatively light (for its capacity) and one person could easily load it on the antenna.

The helium transfer system is shown in Fig. 12. The transfer line was flexible, so that it could be easily connected to the storage containers on the lower end (this starts the transfer) and easily inserted into the maser dewar on the other (after the line was very cold). The liquid was pumped by storage container back pressure. The rate of liquid flow into the line was monitored by watching the scale weight, and the boil-off rate was monitored by watching the flow meter. If these readings were abnormal the transfer was stopped (by disconnecting from the storage container) to find the source of trouble. Otherwise, the transfer was continued until the scale reached a predetermined cutoff weight.

The cutoff weight was a function of the initial weight of the container and the length of time it was desired to operate the maser. The operating times for different quantities of liquid (from the storage container) are

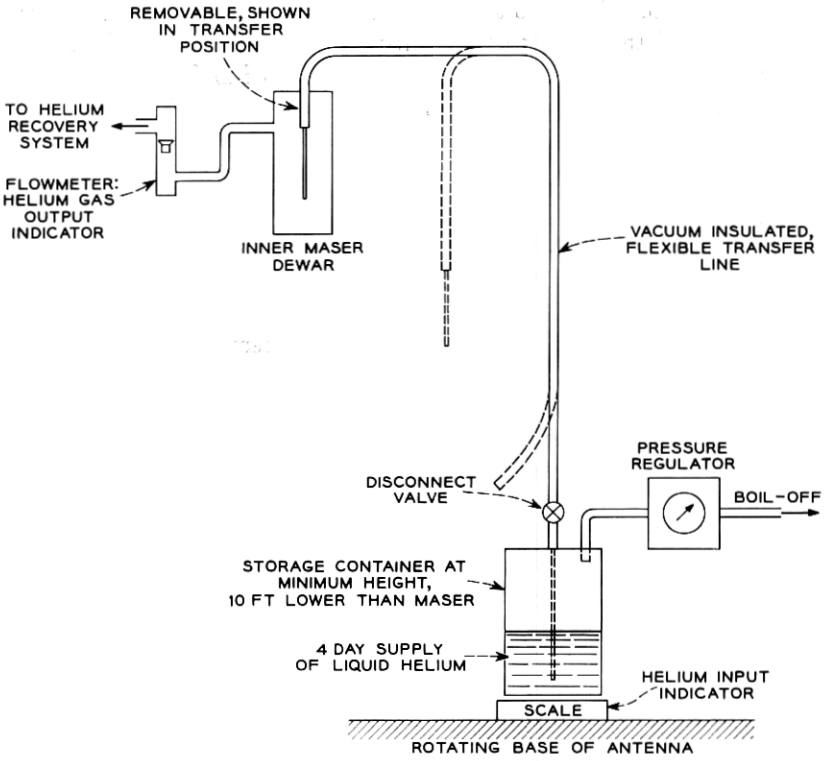

Fig. 12 — Liquid helium transfer system.

shown in Fig. 13. As can be seen, these are also a function of the initial temperature of the dewar. The maximum operating time was over 18 hours, well in excess of the 12 hours required for a series of Echo passes. For daily transfers 12 hours could be obtained using only 14 liters of liquid. The normal objective, which included a 1-liter safety factor, was 15 liters. Since the corresponding weight was $4\frac{1}{4}$ pounds, the normal cutoff weight of the storage container was selected to be about $4\frac{1}{4}$ pounds less than its initial weight.

After the transfer was completed the transfer tube was removed from the maser (to eliminate the tube as a heat leak), and the aperture was sealed with a stopper. The liquid helium in the maser dewar was then "pumped down" (with a vacuum pump) to reduce the maser temperature still further. The pressure declined smoothly until the "lambda" pressure was reached; it then declined at a much slower rate. By noting

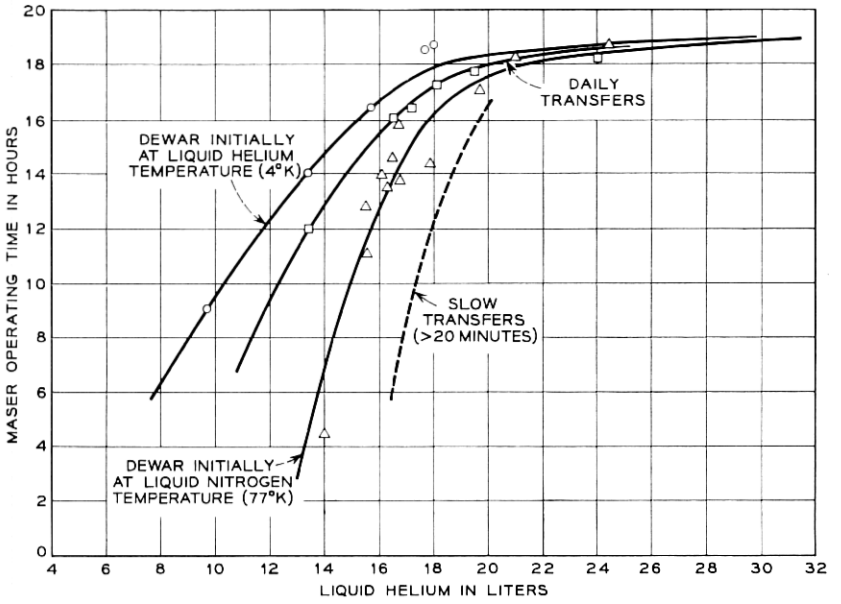

Fig. 13 — Liquid helium required vs. maser operating time.

the time from the start of the pump down to the lambda point and comparing this with previous data, the maser running time could be reliably predicted to within a half hour or so. The vacuum pump, incidentally, was located at the base of the antenna in order to rid the cab of its noise and vibration.

Since the receiver was planned during a period of helium shortage, a gas recovery system was included as a conservation measure. The boil-off from the helium transfer and the exhaust from the vacuum pump were piped to the recovery system (in a nearby building) via a rotating joint on the vertical axis of the antenna mount. Although the integrated boil-off rate exceeded the storage and compression capacity by a large factor, the excess time was short, and 75 per cent of the available gas could be recovered and purified.

REFERENCES

1. Ruthroff, C. L., and Jakes, W. C., Jr., System Calculations, this issue, p. 1029.
2. Ruthroff, C. L., FM Demodulator with Negative Feedback, this issue, p. 1149.
3. DeGrasse, R. W., Hogg, D. C., Ohm, E. A., and Scovil, H. E. D., Ultra-Low-Noise Antenna and Receiver Combination for Satellite or Space Communication, Proc. Nat. Elect. Conf., **15**, 1959, p. 370.

4. Jakes, W. C., Jr., Participation of Bell Telephone Laboratories in Project Echo and Experimental Results, this issue, p. 975.
5. Crawford, A. B., Hogg, D. C., and Hunt, L. E., A Horn-Reflector Antenna for Space Communication, this issue, p. 1095.
6. Schelkunoff, S. A., *Electromagnetic Waves*, D. Van Nostrand Co., New York, 1957, pp. 269, 260, 390, 327.
7. Mumford, W. W., unpublished manuscript.
8. Bolinder, E. F., Fourier Transforms in the Theory of Inhomogeneous Transmission Lines, Trans. Royal Inst. Tech., Stockholm, No. 48, 1948.
9. Beck, A. C., and Dawson, R. W., Conductivity Measurements at Microwave Frequencies, Proc. I.R.E., **38,** 1950, p. 1181.
10. DeGrasse, R. W., Kostelnick, J. J., and Scovil, H. E. D., 2390-mc Traveling-Wave Masers, this issue, p. 1117.
11. Kibler, L. U., Standby Receiver System, this issue, p. 1129.
12. White, W. D., and Greene, J. G., On the Effective Noise Temperature of Gas Discharge Noise Generators, Proc. I.R.E., **44,** 1956, p. 939.
13. Hogg, D. C., Effective Antenna Temperatures Due to Oxygen and Water Vapor in the Atmosphere, J. Appl. Phys., **30,** 1959, p. 1417.